Accurate and Wide Field of View MEMS-based Sun Sensor for Industrial Applications

Abstract **- This paper shows the design, fabrication, simulation results and experimental results of an improved miniaturized two-axis sun sensor for industrial applications, by adapting the technology used previously in satellite applications. The sensor for each axis is made of six photodiodes integrated in a crystalline silicon substrate, and a layer of cover glass, which is used to protect the silicon and to hold the windows. The high precision will be obtained by the subdivision of field of view (FOV), which is ±60º, with a resolution of 0.1º. Each region will be controlled by an independent high precision solar sensor. The sensor can be used for sun tracking applications in photovoltaic system, heliostat concentration and lighting purposes.**

Index terms **– Microelectromechanical system (MEMS), photodiodes, microsensors, angle measurement, sun-tracking**

1. INTRODUCTION

A solar sensor is a device widely used in an attitude control of satellites [1]-[3]. The accurate relative position of the satellite to the sun is obtained from the incidence angle measurement of the sun light beam [4]. Recently, this kind of sensors is being used for terrestrial applications on industrial environment, such as solar power plants, photovoltaic energy generation, energy efficiency improvement and lighting in buildings [5]-[7].
We have developed a MEMS based sun sensor (Vectorsol, Fig. 1) for satellite application with a 0.15º accuracy and a ±60º field of view (FOV).

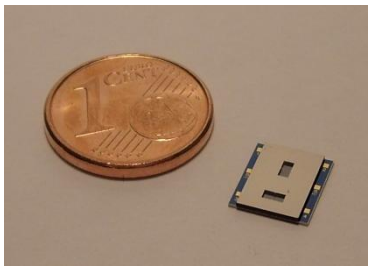

Figure 1. Vectorsol sensor.

The resulting device has been boarded in the Spanish nano satellite NANOSAT-1B, which was launched in July 2009 and it has been working at expected performance since then [8][9]. Fig. 2 shows the final sun sensor device, which has been protected using a cover glass and [10] encapsulated using an aluminum shell.

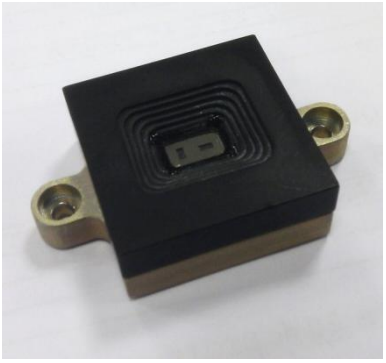

Figure 2. Sun sensor device for satellite application.

The technology used in this sun sensor doesn't allow improving both accuracy and FOV simultaneously. Better the accuracy narrower the field of view due to geometrical reasons. New terrestrial applications require better properties in accuracy without harming FOV, so a new sensor development is needed.
To reach that target is essential to maintain high gain factor and to reduce quantification errors in AD converters. A way to achieve these specifications is using subdivision of the FOV (Fig. 3) [12][13].

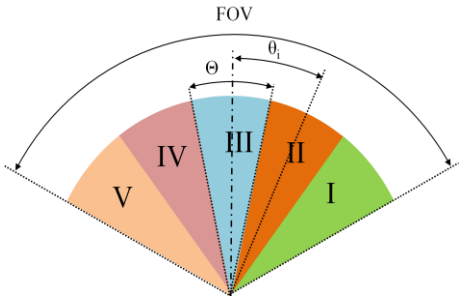

Figure 3. Subdivision of the FOV.

A first prototype of sun sensor using this design rule was manufactured and tested. This sensor achieved the accuracy searched, but only in a very specific region of the FOV. Due to internal reflections, secondary light beams reached external photodiodes, which implied several irregularities on the graphs. Therefore, it was impossible to achieve the objective in the full range of FOV.
Based on the good results obtained with Vectorsol, and using the concept of subdivision of the FOV, a new design is presented: µFineSunSensor (µFSS). Subdivision of the FOV will be used, but each region will be controlled by an independent Vectorsol sensor.
The objective of this work is, therefore, the design, fabrication and characterization of the µFineSunSensor and the adaptation of this technology to industrial applications. The new sun sensor has been applied to sun tracking system and results are compared with traditional solutions.

2. THEORY, MODELLING AND SIMULATION

A. Sensor Principle

The new design is based in the structure of Vectorsol. (Fig. 4). The sun rays reach two photodiodes trough a cover glass with an upper window, and generate a current in each one. The incidence angle of the incoming ray can be obtained from the currents ratio generated in both photodiodes.

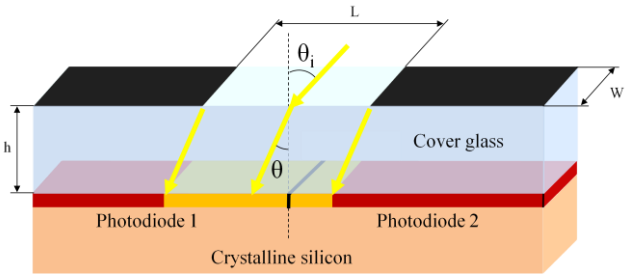

Figure 4. One axis sun sensor structure.

As the illuminated areas of the photodiodes are proportional to current generated by them (Fig. 5) it is possible to determine the angle of incidence using the normalized function R, given by equations (1).

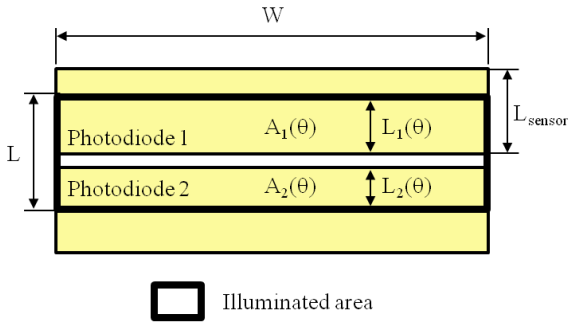

Figure 5. Illuminated area in photodiodes.

$$R(\theta) = \frac{I_{ph_2} - I_{ph_1}}{I_{ph_2} + I_{ph_1}} = \frac{A_2(\theta) - A_1(\theta)}{A_2(\theta) + A_1(\theta)} = \frac{L_2(\theta) - L_1(\theta)}{L_2(\theta) + L_1(\theta)} \quad (1)$$

Where $L_1 \cdot W$ and $L_2 \cdot W$ are the illuminated area of the photodiodes 1 and 2, respectively. The normalized function guarantees the independence of R with the radiation intensity.

Based on this design, it is possible to manufacture a more accurate sensor by increasing the height of the glass. Displacement of the beam in the silicon is directly proportional to the height h of the glass, as it can be seen in (2) and Fig. 6.

$$x = 2h \cdot \tan\left(\frac{\Delta\alpha'}{2}\right) = 2h \cdot \tan\left[\arcsin\left(\frac{n_1}{n_2} \cdot \sin\left(\frac{\Delta\alpha}{2}\right)\right)\right] \quad (2)$$

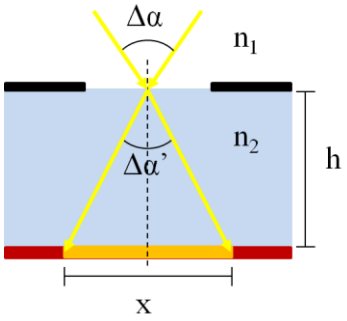

Figure 6. Projection of the beam in the silicon.

The entire area of a photodiode is completely covered with a smaller sweep of the incident beam, which makes the sensor more sensitive to increases of the incident angle (Fig. 7).

On the other hand, increase the sensitivity implies decrease the FOV: one single sensor is capable to see only a narrow region. The complete FOV will be reached by adding in serial of so many sensors as needed.

In order to obtain complementary regions of the FOV, it is necessary to modify the central angle of the same sensors (the incidence angle of the incoming ray in which both photodiodes are equally illuminated). To achieve this, the upper window is displaced (Fig. 8). The relationship between displacement (Δ) and central angle (θ_c) is given by equations (3).

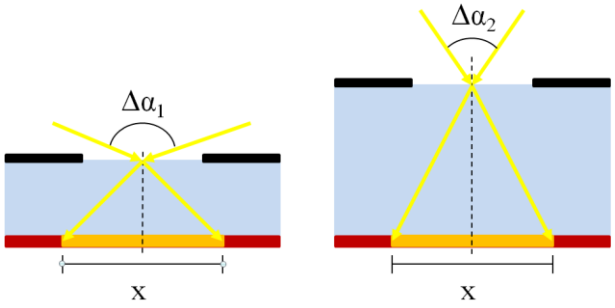

Figure 7. Sensor sensitivity as a function of the height of the glass.

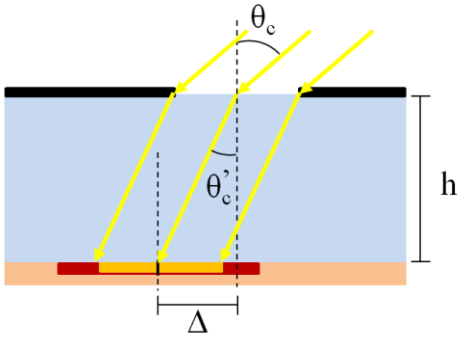

Figure 8. Displacement of the window.

$$\theta_c = \arcsin\left[\frac{n_2}{n_1}\sin\left(\arctan\left(\frac{\Delta}{h}\right)\right)\right] \quad (3)$$

B. Fine sun sensor design

Table 1 shows the characteristics of a one axis μFSS, composed of six photodiodes. These photodiodes have been dimensioned to make three independent sensors which

measure the incidence angle in different regions (Fig. 9). The resulting FOV is the sum of the three independent regions.

FOV	120º (±60º)
Regions	3 (40º each)
Number of photodiodes	6
Central angles	-40º, 0º, 40º
Height of the glass	1.75 mm
Size of the window (WxL)	1.4x1.7 mm^2
Size of the photodiodes (W_sxL)	4.4x1.7 mm^2

Table 1. µFineSunSensor characteristics.

The width of the photodiodes (W_s) is 3 mm bigger than the width of the window (W) in order to assure the independence between the two axes: variations of the angle in one axis illuminate the same area in photodiodes of the other axis sensor.

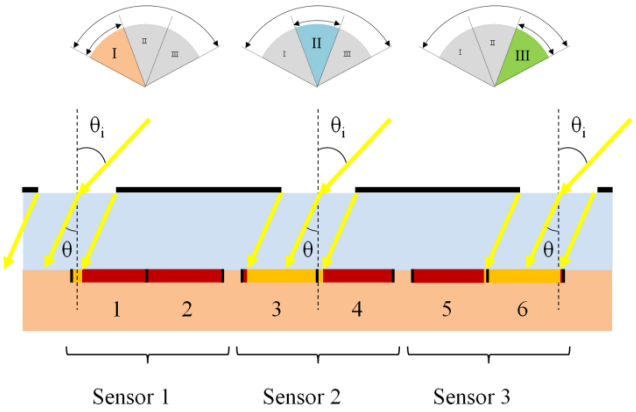

Figure 9. One axis µFineSunSensor structure.

The final device consists of two structures like this placed orthogonally, in order to get the angle of incidence in both axes and the light source completely localized.

B. Device modeling and simulation

The layout of a one axis sun sensor can be seen in Fig. 10. The gap between each pair of photodiodes is enough to not interfere with each other. The red zone is the active area of the photodiodes, and the pink ones are the orthogonal projection of the three windows in the silicon. The generated photocurrents are collected from the pads, represented by the yellow squares.
The photodiodes have been oversized. The FOV of each sensor has been increased from 40º to 80º, in order to work in the central region of the R functions and assure a lineal behavior in all the operating range. This implies that the regions in the FOV overlap between them. The discrimination of the best angle measurement will be made by software processing.
Fig. 11 shows the results of the simulation of the sensor using Matlab. The effective illuminated area for each photodiode as a function of incident angles for both axes is represented in these figures, as well as the R functions of the three regions. Internal reflections have been considered. Generated photocurrents are proportional to the illuminated area, so the expected experimental results will be a scaled version of these simulations.
Some irregularities can be seen. Due to the reflections, the R functions present a certain curvature in the central region, so there is not a completely independence between axes. This effect can be identified and neglected on the calibration of the device.

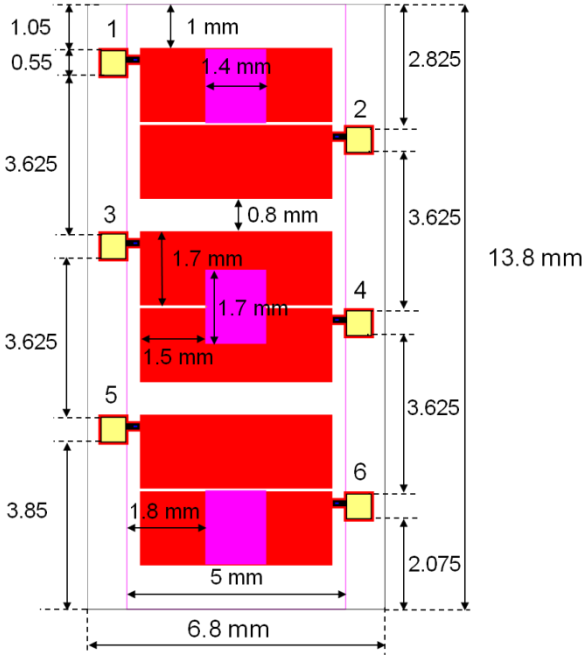

Figure 10. One axis sensor layout.

3. SENSOR CHARACTERIZATION AND FABRICATION

The fabrication of the silicon device and the cover glass has been done in the Laboratory of the MNT group of the UPC. The sensor fabrication combines microelectronics and MEMS standard processes and high efficiency solar cells manufacturing techniques used by MNT group [11]. Bonding and final device implementation has been done in the facilities of the Microsystems Group of the University of Seville.

A. Silicon die fabrication

The silicon die has been fabricated using Fz p-type crystalline silicon 4 inch double side polished wafers. As seen in Fig. 12, the fabrication process has had the followings steps: a) Thermal oxidation at 1060ºC, t=240 min. b) Definition of the emitter regions (N+ regions) of the six photodiodes using standard photolithography, TMAH etching and phosphorus diffusion, T=870ºC, t=30 min. c) SiO_2 etching at the front and rear surfaces. d) SiO_2 passivation T=1060ºC, t=80 min. e) Emitter contacts in N+ regions defined by photolithography and SiO_2 etching. f) Ti/Pt metallization using sputtering and lift-off technique. g) Al metallization in the rear surface and thermal annealing, T=400ºC, t=15 min. h) Au metallization in pads and thermal annealing, T=460ºC, t=10 min. i) Finally, laser-fired contacts in rear surface (18A, one pass, 40 mm/s, 8 kHz).

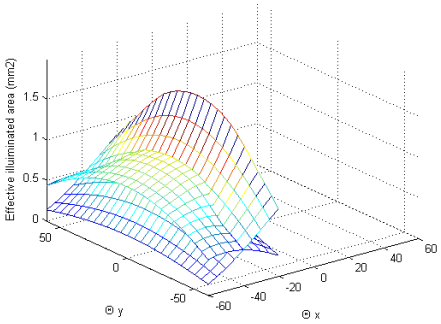

a)

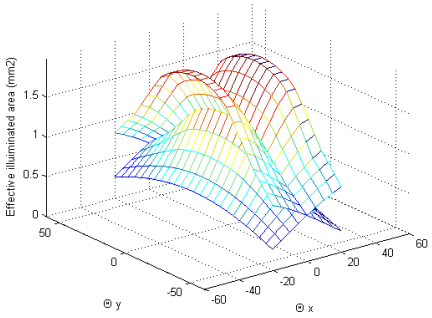

b)

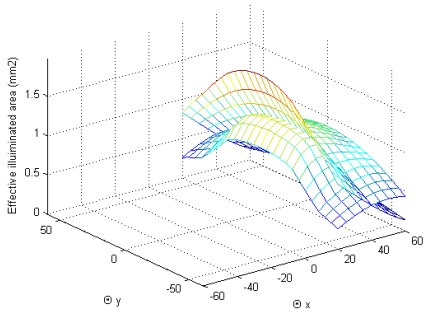

c)

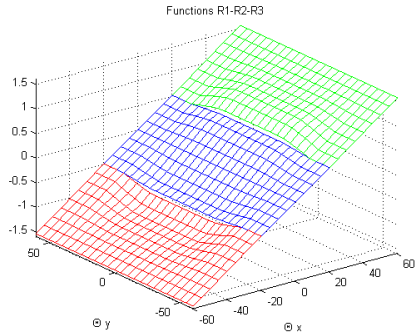

d)

Figure 11. Theoretical effective illuminated area in photodiodes 1-2 (a), 3-4 (b) and 5-6 (c), and *R* functions (d).

B. Cover glass metallization

An uncoated cover glass 4" wafers of 1.75 mm thickness has been used to implement the windows and the cavity. The cover glass metallization has been made as follows: a) Photoresist deposition at the front side (7 μm) and lithography. b) Al metallization using sputtering technique. c) Metal patterning using lift-off technique.

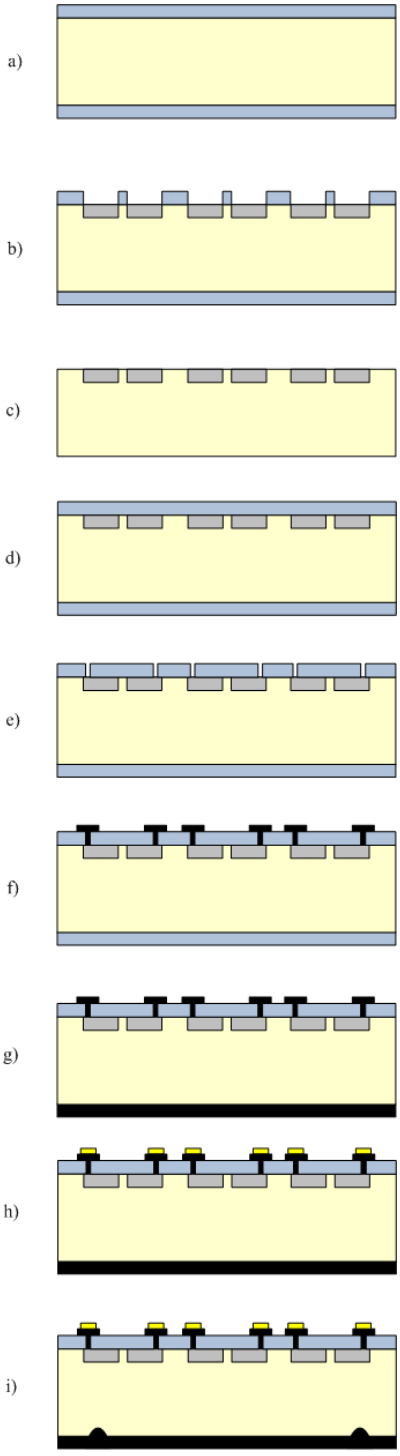

Figure 12. Main stages in the silicon die fabrication.

C. Bonding and implementation

To bond cover glass with silicon the glue bonding technique has been used. A transparent and non-conductive epoxy was deposited carefully in four peripheral points to avoid covering the electrodes and windows. Fig. 13 shows the fabricated device (silicon and cover glass).

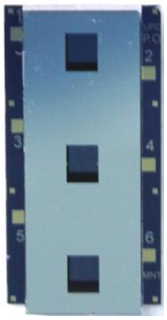

Figure 13. One axis fabricated device.

Two of these devices are placed orthogonally in a PCB board (Fig. 14). The contacts of the common anode of the photodiodes are placed in the rear surface of the silicon, so in order to bond silicon and PCB a conductive epoxy is used. The electrical connection of the cathodes with the PCB board is made using a wire bonding process.

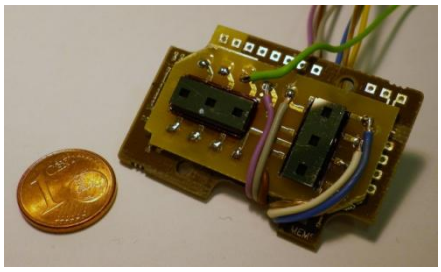

Figure 14. Fabricated two axis high precision solar sensor.

E. Circuits

The signal adaptation circuit used in the device can be seen in Fig. 15. The signals of the sensors are multiplexed, due to the elevated number of photodiodes on this design in comparison with the original Vectorsol. An operational amplifier is added to de design, used as voltage follower, in order to provide infinite impedance and to make the output signal independent from the measurement instrument. The relationship between generated photocurrent (I_d) and output voltage (V_o) is given by equation (4).

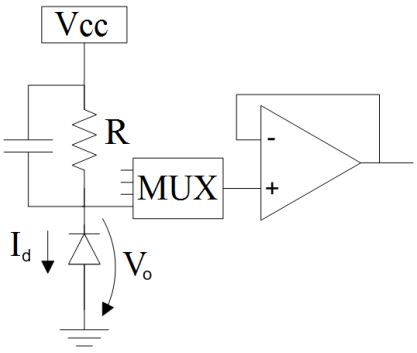

Figure 15 Signal adaptation circuit.

$$V_o = V_{cc} - I_d \cdot R \qquad (4)$$

F. Calibration set-up

The calibration system used in the experiments consists of a solar simulator and two motorized rotary stages placed orthogonally for control of both axes (Fig. 16). An aluminum structure, black anodized in order to avoid reflections, supports all the equipment. The sensor is placed just in the center of the rotation, being always illuminated by the beam generated in the solar simulator.

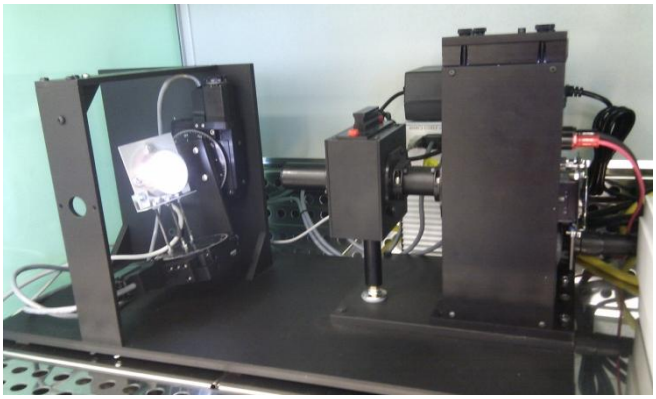

Figure 16. Calibration system set-up.

The model of the solar simulator is Sciencetech SF150 Collimated Solar Simulator. With a 150W (ozone free) xenon lamp and 2" optics it can produce a collimated class A uniformity 1 Sun beam up to 1.5" diameter. It has two filters, AM0 and AM1.5G, for spatial and terrestrial radiation generation.
The motorized rotary stages are the 8MR191 from Standa, with a rotation range of 360º and a resolution of 0.01º. They are controlled by a USB 8SMC1-USBh-B2 controller, and all the software used in the experiments is programmed with LabVIEW.

4. EXPERIMENTAL RESULTS

A calibration of ±60º with a 5º steps in both axes has been done, as shown in Fig. 17. The generated photocurrent in each photodiode as a function of incident angles for both axes is represented, as well as the R functions for each region.
As expected, the shape of the plots is quite similar to the simulations.
By combining the R functions of the two axes, it is possible to obtain the inverse functions ($\theta_{x,y} = f(R_{1,2,3}, R_{4,5,6})$). Once the sensor is calibrated, it calculates the value of R in both axes (using the photocurrents given by the photodiodes) and applies it in the inverse functions, providing to the user the value of angular position. In Fig. 18 it can be seen the inverse functions for the central region ($\theta_{x,y} = f(R_2, R_5)$). In addition, the interpolated surfaces (used to obtain angles between calibration points) are represented in the plots.
Once the calibration curve is obtained it is necessary a verification process. The sensor response for 64 random positions in each region are captured and compared with the real angles provided by the rotary stages. The 3σ value in the 9 regions (3x3) is shown in Table 2. The numeration used for the regions can be seen in Fig. 19. A mismatching between cover glass and silicon in y axis is appreciated in the prototype, leading to bad results in regions 7, 8 and 9.

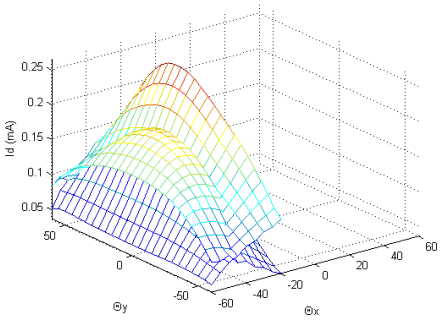

a)

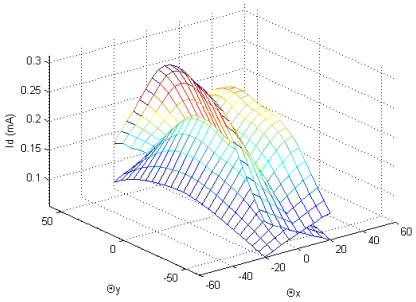

b)

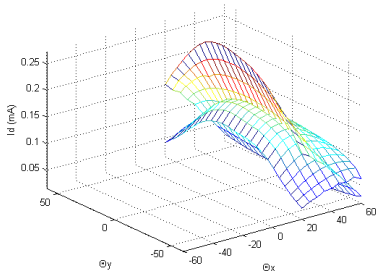

c)

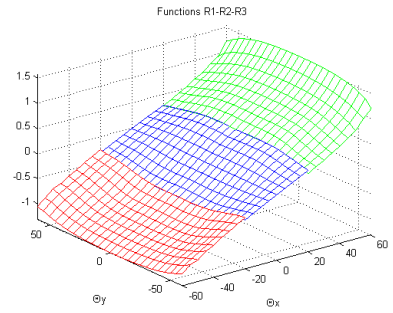

d)

Figure 17. Generated currents in photodiodes 1-2 (a), 3-4 (b) and 5-6 (c), and *R* functions (d).

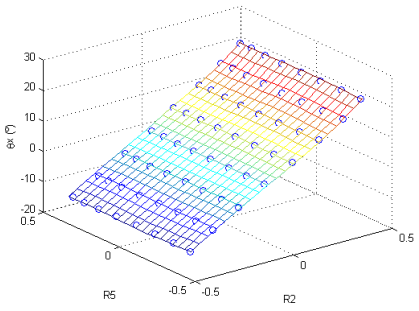

a)

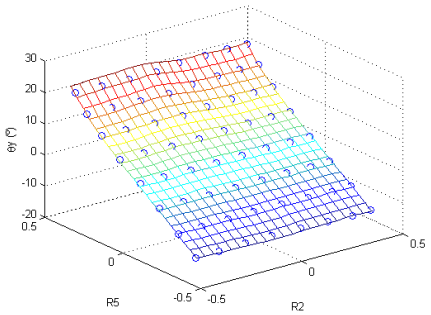

b)

Figure 18. Inverse functions in the central region of *x* axis (a) and *y* axis (b).

Region	3σ (X axis)	3σ (Y axis)
1	0.092	0.144
2	0.049	0.09
3	0.14	0.221
4	0.029	0.052
5	0.026	0.042
6	0.032	0.053
7	0.2118	0.94
8	0.513	2.03
9	0.489	1.128

Table 2. 3σ values for both axes in all the FOV.

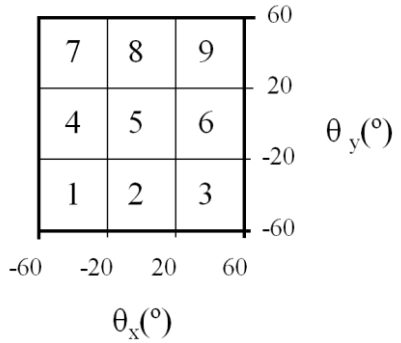

Figure 19. Numeration of the regions.

5. APPLICATIONS

A. Sun tracking

The energy market, specifically solar energy, is on constant evolution, searching higher energy efficiency and cost reduction. One of the most important factors to achieve this is the solar tracking. Currently, mathematical algorithms [14] or large and heavy sun sensors are used to find the position of the sun. µFineSunSensor is smaller and have lower power consumption than such sensors and allows a close-loop control of tracking. This sensor, combined with a structure holding a big mirror, can be used for illuminate surfaces such as buildings shadow fronts, large windows and inner courtyards, leading to a better use of natural light. These structures can be also used like solar tracker for photovoltaic systems or heliostat concentration without modifications. Figure 20 shows one of these structures, which has been built in the roof of the Escuela Superior de Ingenieros of Seville and it is used for lighting purpose. The

target was located 80 meters away from the mirror. The sun sensor was placed between the mirror and the target, and a control application was developed to close the loop with the signal received from the sun sensor.
Both the sensor and the mirror structure have been working at expected performance since the construction of the sun tracker. The mirror orientation was continuously adapting to the sun movement and the light spot deviation has been less than 20 cm. This deviation is equivalent to an accuracy of 0.14º and is enough for this kind of applications. The lighting system may be easily installed and orientated to a new target, so we can say that this system is plug and play.
Accuracy of this system is limited by the strength of the mechanical structure and the resolution of the motors. On the other hand, by using this sensors and closing the loop, it is possible to improve accuracy in low cost sun-tracker systems like this one.

Figure 20. Sun tracker based on µFineSunSensor.

B. Satellite applications

The technology in µFineSunSensor is the same used in Vectorsol, which has been already tested and approved for satellite integration [8][9]. By calibrating the sensor with spatial radiation (AM0), the device will be ready for being used in satellite applications. A special package for µFineSunSensor is being designed to undergo the very exigent standards in aerospace area. This sensor will allow to measure the sun position with higher accuracy and more linear response in the whole range of FOV than its predecessor Vectorsol. µFineSunSensor will be boarded in future Seosat Spanish satellite as scientific payload, and first experimental results are expected in 2014.

6. CONCLUSION

This paper shows the design, fabrication and characterization of a high precision solar sensor based on the subdivision of the FOV. Small size and low power consumption has been the principal objectives. Simulation and experimental results has been shown, as well as the terrestrial and spatial applications. A sun FOV of ±60º and angle accuracy better than 0.1º in almost all the FOV (which is actually being improved) is obtained.
One of these sensors will be on board of Seosat satellite from INTA, which is planned to be launched on 2014.
A future work could be the integration of the sensor and the auxiliary circuits of signal adaptation in the same bulk, leading to a much smaller final device than actual.

REFERENCES

[1] X. Lafontan, F. Pressecq, F. Beaudoin, S. Rigo, M. Dardarlhon, J. L. Roux, P. Schmitt, J. Kuchenbecker, B. Baradat, D. Lellouchi, C. Le Touze, J. M. Nicot. “The advent of MEMS in space. Microelectronics Reliability”, vol. 43, Issue 7, (2003) 1061-1083
[2] J. H. Hales and M. Pedersen, “Two-axis MOEMS sun sensor for pico satellites,” in Proc. 16th Annu. AIAA/USU Conf. Small Satellites, Logan, UT, Aug. 2002, pp. 1–12.
[3] T. Böhnke, M. Edoff, and L. Stenmark, “Development of a MOEMS sun sensor for space applications,” Sens. Actuators A: Phys., vol. 130–131, pp. 28–36, 2006.
[4] Young-Keun Chang, Mi-Yeon Yun, Byung-Hoon Lee. “A new modelling and validation of two-axis miniature fine sun sensor”. Sensors and Actuators A, 134 (2007), 357-365.
[5] J. M. Quero, C. Aracil, L. G. Franquelo, J. Ricart, P. R. Ortega, M. Dominguez, L. Castañer, and R. Osuna, “Tracking control system using an incident radiation angle microsensor,” IEEE Trans. Ind. Electron., vol. 54, no. 2, pp. 1207–1215, Apr. 2007.
[6] D. Y. Goswami, S. Vijayaraghavan, S. Lu, and G. Tamm, “New and emerging developments in solar energy,” Sol. Energy, vol. 76, no. 1, pp. 33–43, Jan.–Mar. 2004.
[7] T. M. Razykov, “Photovoltaic solar electricity: State of the art and future prospects,” in Proc. 6th ICEMS, Nov. 9–11, 2003, vol. 1, pp. 297–301.
[8] J. García Ortega, C.L. Tarrida, J.M. Quero, F.J. Delgado, P. Ortega, L. Castañer, M. Reina, M. Angulo, Y. Morilla, J. García. “MEMS solar sensor testing for satellite applications”, Proc. of the 7th Spanish Conference on Electron Devices CDE-09, Santiago de Compostela, Spain, Feb. 11-13, 2009.
[9] P. Ortega, G. Lopez, J. Ricart, M. Dominguez, L. Castañer, J.M. Quero, C.L. Tarrida, J. García. “Fabrication of a miniaturized two axis sun sensor for satellite applications”. IEEE Sensors Journal, vol 10, nº10, pgs. 1623-1632, Oct. 2010.
[10] J. Rusell, G. Jones, and J. Hall, “A new UVR/IRR coverglass for triple junction cells,” in Proc. 4th IEEE World Conf. Photovoltaic Energy Conversion, Waikoloa, HI, May 2006, pp. 1911–1914.
[11] P. Ortega, S. Bermejo, and L. Castañer, “High voltage photovoltaic mini-modules,” Progress in Photovoltaics: Res., vol. 16, pp. 369–377, 2008.
[12] F. J. Delgado, P. Ortega, C. L. Tarrida, J. García, M. Angulo, J. M. Quero, “A New Design of High Precision Solar Microsensor for Satellite Applications”, Proc. of the 9th IEEE Conference on Sensors, Waikoloa, Hawaii, Nov. 1-4, 2010.
[13] F. J. Delgado, J. García, C. L. Tarrida, J. M. Quero, “Fabrication of a MEMS based high precision solar sensor for satellite applications using CMOS technology”, Proc. of the 8th Spanish Conference on Electron Devices CDE-11, Palma de Mallorca, Spain, Feb. 9-11, 2011.
[14] J. J. Michalsky, “The astronomical almanac’s algorithm for approximate solar position (1950–2050),” Sol. Energy, vol. 40, no. 3, pp. 227–235, Jun. 1988.